# Variations of the Geometries and Band Gaps of Single-Walled Carbon Nanotubes and the Effect of Charge Injection

**Guangyu Sun,[†,‡] Jenö Kürti,[†,§] Miklos Kertesz,*[,†] and Ray H. Baughman[||]**

*Department of Chemistry, Georgetown University, Washington, D.C. 20057, Department of Biological Physics, Eötvös University, Budapest, Hungary, and Department of Chemistry and NanoTech Institute, University of Texas at Dallas, Richardson, Texas 75080*

*Received: December 19, 2002; In Final Form: May 5, 2003*

The geometries of neutral and charged carbon single-walled nanotubes (SWNTs) have been calculated using density functional theory. Periodic boundary conditions, a plane wave basis, and ultrasoft pseudopotentials are used in the generalized gradient approximation for isolated SWNTs with diameters of up to 20 and 12.5 Å for armchair and zigzag nanotubes, respectively. Two different bond lengths and two different bond angles are present in these SWNTs. The largest calculated difference in these bond distances is 0.05 Å, which is obtained for a small-diameter zigzag nanotube. The largest deviation from graphitic bond distances is 0.03 Å for the zigzag series and 0.008 Å for the armchair series. Interesting oscillations in bond lengths and nanotube repeat lengths, but not bond angles, are predicted as a function of $n - m$ for $(n, m)$ nanotubes. These oscillations have a periodicity of 3. The band gap of semiconducting tubes first tends to increase and then decrease with increasing nanotube diameter. The largest calculated band gap is found to be around 1.1 eV. Different zigzag nanotubes with $n = 3i$, $3i + 1$ and $3i + 2$ show different dimensional changes upon the injection of small charge (0.01 e per carbon atom), and the dimensional changes approach that of graphite when the tube diameter increases.

## Introduction

Single-walled carbon nanotubes (SWNTs), which are structurally related to fullerenes and to graphene (a single graphite sheet), were observed by Iijima in 1991 using transmission electron microscopy.[1] Neglecting the structure at the ends, which can be either open or closed, these SWNTs can be viewed heuristically as being generated by rolling a graphene sheet to form a seamless carbon nanotube cylinder. The middle section of a nanotube can be well modeled by an infinite tube, where periodic boundary conditions are applicable.[2]

The structures of the rolled-up graphene are characterized by the roll-up vector $(n, m)$, where the indices correspond to a 2D lattice vector ($\mathbf{R} = n\mathbf{a}_1 + m\mathbf{a}_2$) and where $a_1$ and $a_2$ are equivalent lattice vectors of graphene.[2] The diameter of the resulting tube is approximately

$$D = \frac{a[3(n^2 + nm + m^2)]^{0.5}}{\pi} \qquad (1)$$

where $a = 1.42$ Å. Two types of SWNTs, characterized by the roll-up vector of $(n, n)$ and $(n, 0)$, have simple translational symmetry, and these are referred to as armchair and zigzag nanotubes, respectively, corresponding to the patterns of hexagons around the nanotube belt. Figure 1a illustrates one example for each of the two types: (5, 5) and (10, 0). According to Hückel (or simple tight-binding) theory, SWNTs have a nonzero band gap and are semiconducting unless $(n - m)/3$ is an integer, in which case they are metallic.[2] Although the 3D structures of SWNTs are different from that of graphene, their covalent connectivities and bonding are very similar. This leads to the expectation that the CC bonding in SWNTs should be similar to that of graphene, at least when the nanotube diameter is large. All $(n, n)$ armchair tubes and all $(n = 3i, 0)$ zigzag tubes are metallic at the Hückel level of theory (where $i$ is an integer), and the $(n = 3i + 1, 0)$ and $(n = 3i + 2, 0)$ zigzag

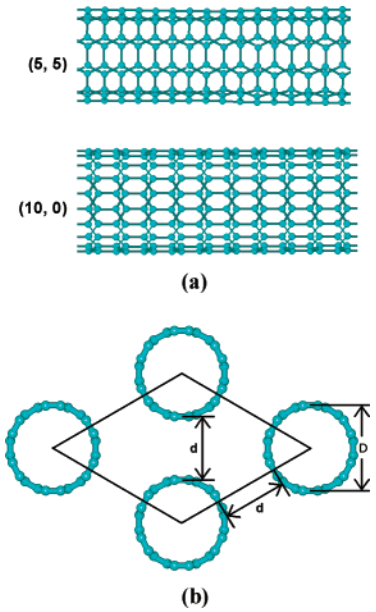


**Figure 1.** (a) Ball-and-stick rendering of an armchair (5, 5) nanotube and a zigzag (10, 0) nanotube. (b) Cross section of the hexagonal unit cells used in this study for the majority of the single-walled carbon nanotubes. Some calculations used tetragonal unit cells.

* Corresponding author. E-mail: kertesz@georgetown.edu.
† Georgetown University.
‡ Present address: Laboratory of Medicinal Chemistry, NCI−Frederick, NIH, 376 Boyles Street, Frederick, MD 21702.
§ Eötvös University.
|| University of Texas at Dallas.

10.1021/jp022629p CCC: $25.00 
Published on Web 06/27/2003

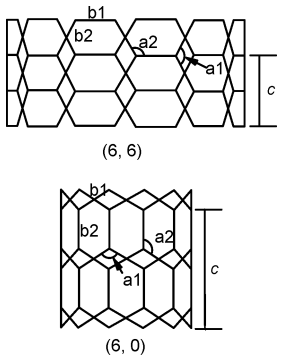


**Figure 2.** Definition of bonds (*b*1 and *b*2), bond angles (*a*1 and *a*2), and unit cell lengths (*c*) in an armchair (6, 6) and a zigzag (6, 0) nanotube. *c* is parallel to the tube axis.

tubes are expected to be semiconducting. For very large nanotube diameters (*n* values), the chemical bonding is expected to approach that in a single graphene sheet. Here we explore the significant deviations from graphenelike behavior for small values of *n*.

The geometries of zigzag SWNTs (for $n = 5$ to 12) were recently calculated using the local density approximation (LDA).[3] Clear differences were predicted between the lengths of the two types of bonds in the zigzag tubes (Figure 2), with *b*1 bonds being slightly longer and *b*2 bonds being slightly shorter than those in graphene. Hence, the longest bonds are those that are most nearly orthogonal to the nanotube axis. These differences in bond lengths were shown in ref 3 to diminish with increasing tube diameter, approaching the graphene values from below and from above roughly as $1/D^2$, where *D* is the nanotube diameter.

In this paper, we study the systematic variations of carbon−carbon bond lengths as a function of the nanotube diameter for three charge states: neutral and uniformly charged SWNTs with a charge value of $q = \pm 0.01e$ per carbon. Here the nanotubes are studied for *n* values between 5 and 16 for both (*n*, *n*) armchair and (*n*, 0) zigzag nanotubes. We have discovered a periodicity (as a function of *n*) in the geometrical changes for the zigzag family, which was not noticed in the earlier LDA study.[3] We also describe features of the electronic structures of small-diameter semiconducting nanotubes that are significantly different from the predictions of tight-binding theory and compare these results with previous LDA calculations by Blase et al.,[4] Reich et al.,[5] and Kanamitsu and Saito.[3] Because we extended the calculations to larger-diameter members of the series, we were able to find nanotubes that begin approaching graphenelike dimensions. We then report the dimensional changes (strain) in both armchair and zigzag nanotubes with small to medium diameters upon charge injection. Finally, all of the predicted geometrical, electronic, and strain behavior of armchair nanotubes and zigzag nanotubes with different index *n* values is attributed to their different electronic structures.

## Computational Method

Geometry optimizations for SWNTs used density functional theory in the generalized gradient approximation (GGA). The Perdew−Wang 91 (PW91) GGA functional[6] was used in all calculations in combination with ultrasoft Vanderbilt-type pseudopotentials[7] generated for the PW91 exchange-correlation functional. Calculations were performed using the Vienna ab initio Simulation Package (VASP v.4.4.2), which is a plane wave, solid-state program.[8,9] The VASP code has been validated for structures of various organic molecules, including conjugated molecules and molecular ions,[10] graphite and diamond,[11] and SWNTs.[12,13] The VASP program was modified to allow for the relaxation of the unit cell in selected dimensions. (Note that version 4.4.5 of the VASP program now permits this constrained cell relaxation.[14]) Default cutoff energies designated as "medium accuracy" were used (e.g., 290 eV for carbon). Monkhorst−Pack-type *k*-point meshes originating at the Γ point were used. We used the smallest possible unit cell; therefore, there were $4 \times n$ carbon atoms in the unit cell for both (*n*, *n*) and (*n*, 0) SWNTs. Figure 1b illustrates the cross section of the hexagonal unit cells used for the majority of the nanotubes. For nanotubes with $n = 8$ and 10, tetragonal unit cells were used. The *k*-point mesh varied from $1 \times 1 \times 30$ for small-diameter nanotubes to $1 \times 1 \times 24$ (armchair) and $1 \times 1 \times 20$ (zigzag) for the medium-diameter nanotubes and to $1 \times 1 \times 12$ for the largest-diameter nanotubes. Convergence was enhanced by using fractional occupancy generated by Gaussian broadening ($\sigma_{GB} = 0.10$ eV) of the one-electron energy levels. As a result of the Gaussian broadening, the energy levels close to the Fermi level have fractional occupations. We have done a few tests with a smaller $\sigma_{GB}$ value (0.01 eV), resulting in changes of the geometrical parameters by less than 0.001 Å and 0.1° for both neutral and charged SWNTs. This is in agreement with our earlier experience on *trans*-polyacetylene, where $\sigma_{GB} = 0.10$ eV gives results similar to $\sigma_{GB}$ values of 0.03 and 0.01 eV for the medium *k*-point mesh.[15]

Charged nanotube calculations were performed in a "generic" manner in the sense that they are not ion-specific. Only the atoms of the nanotubes were specifically included in these generic calculations; the counterions were represented by a uniform background charge (jellium) required to provide charge neutrality of the unit cell. The additional charge at $q = \pm 0.01e$ per carbon on the carbon networks was introduced by filling the lowest unoccupied orbitals or emptying the highest occupied orbitals. A fixed inter-tube distance of $d = 6$ Å was used (Figure 1b), which is large enough to ensure that the results correspond to isolated tubes.

## Quality of the Predictions and the Band Gap Scaling Factor

In this section, we comment on the quality of the quantitative predictions of the modeling described in the Computational Method section before turning to the new results on the nanotubes. The patterns of bond distance variations from single to double bonds are reliably reproduced with the VASP calculations, and even more subtle variations among conjugated bonds are reproduced reasonably well. A comparison of selected CC bond distance predictions with experiment is provided in ref 10. Overall, variations of CC bond distances are reliably predicted, with the exception of the bond alternation parameter in polyacetylene. This latter problem is a cause of some concern, but its origin is related to the exact exchange term in the Peierls distortion of polyacetylene.[16] Because such a term does not appear to be critical in the electronic structures of SWNTs, we expect the predictions of this paper to be reliable. The calculated bond length in graphene or graphite is 1.419 Å at this level of theory,[13] a value very close to the experimental value (1.42 Å[17]). Other CC bonds lengths predicted by VASP are too short: by 0.004, 0.010, and 0.002 Å for acetylene, ethylene, and ethane, respectively. The differences between observed and calculated bond lengths for graphite and benzene are smaller than 0.002 Å.

Turning to the band gaps, it is widely assumed that the band gaps produced by DFT are too small. A simple scaling factor

**TABLE 1: Optimized Geometrical Parameters for Neutral SWNTs Calculated by DFT[a]**

| (*n*, *n*) | *b*1 | *b*2 | *a*1 | *a*2 | $\Delta_{1,2}$[b] | *c* | *D*[c] | (*n*, 0) | *b*1 | *b*2 | *a*1 | *a*2 | $\Delta_{1,2}$[b] | *c* | *D*[c] |
|---|---|---|---|---|---|---|---|---|---|---|---|---|---|---|---|
| (5, 5) | 1.427 | 1.423 | 119.3 | 118.7 | 0.004 | 2.456 | 6.78 | (5, 0) | 1.451 | 1.402 | 111.4 | 119.7 | 0.049 | 4.242 | 3.91 |
| (6, 6) | 1.427 | 1.423 | 119.2 | 119.3 | 0.004 | 2.455 | 8.14 | (6, 0) | 1.443 | 1.404 | 113.9 | 119.8 | 0.039 | 4.244 | 4.70 |
| (7, 7) | 1.423 | 1.422 | 119.5 | 119.4 | 0.001 | 2.457 | 9.49 | (7, 0) | 1.434 | 1.414 | 115.6 | 119.8 | 0.020 | 4.251 | 5.48 |
| (8, 8) | 1.421 | 1.421 | 119.7 | 119.5 | 0.000 | 2.457 | 10.85 | (8, 0) | 1.433 | 1.412 | 116.7 | 119.8 | 0.021 | 4.248 | 6.26 |
| (9, 9) | 1.425 | 1.422 | 119.4 | 119.8 | 0.003 | 2.455 | 12.2 | (9, 0) | 1.431 | 1.413 | 117.4 | 119.8 | 0.018 | 4.249 | 7.05 |
| (10, 10) | 1.423 | 1.421 | 119.5 | 119.8 | 0.002 | 2.456 | 13.6 | (10, 0) | 1.426 | 1.417 | 117.8 | 119.9 | 0.009 | 4.254 | 7.83 |
| | | | | | | | | (11, 0) | 1.426 | 1.415 | 118.2 | 119.9 | 0.011 | 4.252 | 8.61 |
| (12, 12) | 1.419 | 1.420 | 119.9 | 119.8 | −0.001 | 2.458 | 16.3 | (12, 0) | 1.424 | 1.416 | 118.5 | 119.9 | 0.008 | 4.254 | 9.39 |
| | | | | | | | | (13, 0) | 1.423 | 1.418 | 118.7 | 119.9 | 0.005 | 4.256 | 10.2 |
| | | | | | | | | (14, 0) | 1.425 | 1.417 | 119.1 | 119.9 | 0.008 | 4.252 | 11.0 |
| (15, 15) | 1.423 | 1.420 | 119.7 | 120.0 | 0.003 | 2.456 | 20.3 | (15, 0) | 1.428 | 1.417 | 119.4 | 119.7 | 0.011 | 4.249 | 11.7 |
| | | | | | | | | (16, 0) | 1.422 | 1.418 | 119.2 | 119.9 | 0.004 | 4.255 | 12.5 |
| graphene | 1.419 | 1.419 | 120.0 | 120.0 | 0.000 | 2.458 | ∞ | graphene | 1.419 | 1.419 | 120.0 | 120.0 | 0.000 | 4.257 | ∞ |

[a] DFT (GGA) calculations under the periodic boundary conditions using VASP. Unit cell size *c*, bonds lengths *b*1 and *b*2, bond angles *a*1 and *a*2, and the tube diameter *D* are defined in Figures 1 and 2. Distances are measured in angstroms, and angles, in degrees. The parameters are interrelated by the following equations: $c = 2(b2)\sin(a1/2)$ for armchair and $c = 2(b2) + 2(b1)\cos(180 - a2)$ for zigzag SWNTs. [b] Bond-length difference, $\Delta_{1,2} = b1 - b2$. [c] *D* was estimated from eq 1.

of 1.20 is used throughout this work to obtain calculated band gaps; this factor is based on the comparison of the calculated HOMO−LUMO energy-level difference calculated for the $C_{60}$ fullerene using the present GGA method (1.66 eV) with the observed value (2.0 eV[18]).

### Geometries of SWNTs

The graphenelike symmetry is broken in SWNTs, leading to two inequivalent C−C bonds[2a,12a] in both the armchair and zigzag nanotubes: those that are oriented mainly around the belt and those oriented mainly along the tube axis. The first type is referred to as *b*1, and the second, as *b*2, as illustrated in Figure 2. As we shall see, in almost all cases, $b1 > b2$. Furthermore, the weighted average of the two bond lengths is slightly larger than the graphene value for all zigzag tubes and for most armchair tubes studied here and the average bond length approaches the graphene value with increasing diameter. This lengthening is an expected consequence of bond weakening in a strained carbon network and should diminish with increasing nanotube diameter. Two types of bond angles are also shown in Figure 2. Table 1 and Figure 3 provide the optimized lengths of *b*1 and *b*2 in selected armchair and zigzag nanotubes that were calculated using density functional theory. The bond length difference ($\Delta_{1,2} = b1 - b2$) for each nanotube and the length of the translational vector along the tube axis are also listed in Table 1. The range of these bond length differences is on the order of 0.05 Å, the largest difference occurring for the (5, 0) zigzag nanotube.

In armchair SWNTs, *b*1 and *b*2 are similar in length to each other, differing by a maximum of 0.004 Å, as shown in Figure 3. The lengths of both *b*1 and *b*2 are very close to the bond length (1.42 Å) in graphite. Note that all bonds in graphene are equivalent ($\Delta_{1,2} = 0$). The nonzero value of $\Delta_{1,2}$ in armchair SWNTs is a direct consequence of the finite wrapping of the graphene sheet that generates the tube and breaks the symmetry of the 2D sheet. With increasing diameter, and *n*, the lengths of *b*1 and *b*2 in armchair SWNTs slightly decrease, as shown in Figure 3a. The curvature of the structure has limited effect on the bond lengths in armchair SWNTs.

In zigzag nanotubes, *b*1 is usually significantly longer than *b*2, as shown in Figure 3a. It is interesting that the averages of the lengths of *b*1 and *b*2 in these zigzag nanotubes are rather close to the CC bond length in graphite, 1.42 Å. Both bonds approach the bond length in graphite for large values of *n*.

The difference between *b*1 and *b*2 is largest for smaller-diameter tubes, as shown in Figure 3b. This is not surprising

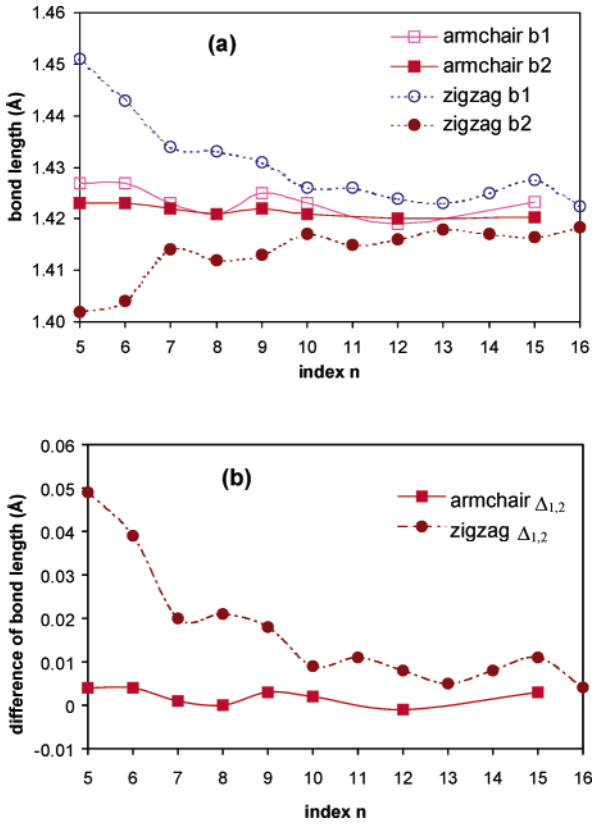


**Figure 3.** Predicted (a) bond lengths and (b) bond length differences between *b*1 and *b*2 for armchair and zigzag nanotubes. Lines connecting the calculated points are provided to show trends.

because as the diameter of the tube increases the structure becomes less constrained. Figure 3b also shows that the zigzag nanotubes have much larger $\Delta_{1,2}$ values than the armchair nanotubes, even after considering the differences in diameter for the same *n* value. When the index *n* increases in zigzag nanotubes, the change in the bond lengths of *b*1 and *b*2 follows a repetitive pattern with a period of 3. For example, four humps can be seen in the $\Delta_{1,2}$ curve for zigzag nanotubes in Figure 3b. These features run from $n = 5-7$, 8−10, 11−13, and 14−16. Similar features can be seen in Figure 3a. Such features were not observed in recent LDA work[3]. Similar periodic features appear for the armchair nanotubes, but the magnitude of the variations is much smaller. On this basis, the zigzag nanotubes can be subdivided into three categories: $n = 3i$, $3i$

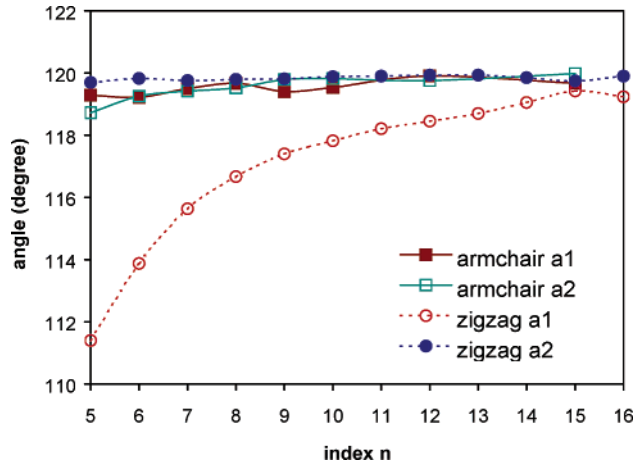


**Figure 4.** Predicted CCC bond angles in armchair and zigzag nanotubes.

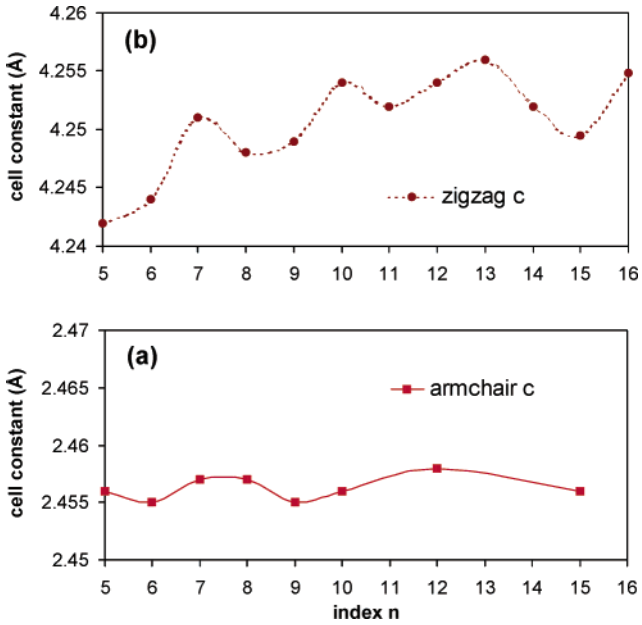


**Figure 5.** Predicted lengths of the translational vectors in (a) armchair nanotubes and (b) zigzag nanotubes. The limiting graphene values are 2.458 and 4.257 Å, respectively.

$+ 1$, and $3i + 2$. We will discuss this further in the context of their electronic structures and band gaps.

The angles in SWNTs deviate from the ideal 120° of the planar honeycomb structure of graphene because of the curvature generated by the roll-up process. Figure 4 shows the predicted values of the two angles in armchair and zigzag SWNTs. For armchair nanotubes, both $a1$ and $a2$ are slightly smaller than 120°. When the diameter of the tubes is increased, the angles gradually approach the ideal 120° value. For zigzag nanotubes, $a1$ is predicted to be 111.4° in (5, 0), which is significantly smaller than the ideal angle of 120° for planar $sp^2$ carbon. When $n$ increases, $a1$ increases gradually toward a limiting value of 120°. However, $a2$ remains close to 120° for all zigzag nanotubes. These observations are consistent with the trend found by Kanamitsu and Saito[3]. The undulations as a function of $n - m$ that are predicted for the bond lengths are not seen for the bond angles.

The length of the translation vector of SWNTs is illustrated in Figure 5. The translation vectors are not independent from the above geometrical parameters and can be determined from the above parameters. For armchair nanotubes, the predicted lengths of the translation vector are close to the ideal value of 2.458 Å in graphene. Because the calculated and experimental bond distances in graphite are very close to 1.420 Å, there is no need to distinguish between the two in this discussion. Small changes in the length of the translation vector are seen when the diameter of armchair nanotubes increases. For zigzag nanotubes, the lengths of the translation vector show larger variations. The length of $c$ is predicted to be 4.242 Å for (5, 0); it gradually increases to 4.255 Å for (16, 0). The length of the translation vector gradually increases when the diameter of the nanotube increases, following an undulating pattern with a period of 3, similar to the pattern of $b2$ in Figure 3. At $n = 7$, 10, 13, and 16, the $c$ values, among the nearby nanotubes, are closest to the corresponding length in graphene, which is $3 \times 1.419 = 4.257$ Å. Note that these values are not fully converged to the graphene value even at $n = 16$. The undulations are related to the electronic structures of the nanotubes, as will be discussed below.

Another aspect of the geometry of SWNTs concerns the curvature. This can be assessed by the $\pi$-orbital axis vector (POAV, $\theta_p$) angle, which measures the pyramidalization of an $sp^2$-hybridized carbon from the planar configuration.[19] The predicted POAV angles for selected nanotubes are (in degrees) (6, 6), $\theta_p = 5.03$; (9, 9), $\theta_p = 3.37$; (12, 12), $\theta_p = 2.48$; (6, 0), $\theta_p = 8.53$; (8, 0), $\theta_p = 6.45$; (10, 0), $\theta_p = 5.18$; and (12, 0), $\theta_p = 4.32$. These values are slightly larger than those reported earlier[20] by only about 0.04°, indicating that the pyramidalization is mostly driven by the curvature of the tubes.

## Electronic Band Structures and Band Gaps

In their classic paper, Mintmire and White described the theoretical trend of diminishing band gaps of SWNTs as a function of increasing diameter.[2b] Deviations from this trend have been noted for small-diameter tubes.[3−5,21] Here we discuss the results of our calculations that are extended over a wider range of nanotubes than those in earlier studies.

Figure 6 shows the predicted electronic band structures of four selected SWNTs, namely, that of the (6, 6) armchair nanotube and those of the (6, 0), (8, 0), and (9, 0) zigzag nanotubes. The calculated band structure for (6, 6) closely resembles the prediction of the tight-binding calculations.[2] Around the Fermi level, both the highest occupied orbital and the lowest unoccupied orbital are nondegenerate. The band crossing at the Fermi level is very close to $k = \pm 2\pi/(3c)$, the crossing point predicted by tight-binding theory. For other armchair nanotubes with $n = 5$, 7, 8, 9, 10, 12, and 15, the predicted band structures are similar to that of the (6, 6) tube.

The $\pi$ and $\pi^*$ part of the predicted band structure of zigzag nanotubes is very similar to the result of the tight-binding method.[2] In the band structures of all zigzag nanotubes, we are able to account for all of the expected $\pi$ and $\pi^*$ bands near the Fermi level. The highest occupied and lowest unoccupied $\pi$ orbitals are both doubly degenerate, and they approach each other at $k = 0$, as shown in Figure 6b−d. The predicted band gaps between $\pi$ and $\pi^*$ bands follow the trend expected from tight-binding theory: very small gaps for $n = 3i$ and large gaps otherwise. The $\pi-\pi^*$ gaps for semiconducting nanotubes tend to decrease with increasing diameter. The main exception to this trend is that the (5, 0) nanotube has a smaller gap than the (7, 0) and (8, 0) nanotubes, which is due to its extremely small diameter.

In the band structures of zigzag nanotubes (5, 0) to (8, 0), a nondegenerate band appears around the Fermi level, and at $k = 0$, the band is below the $\pi^*$ band. This is the lowest

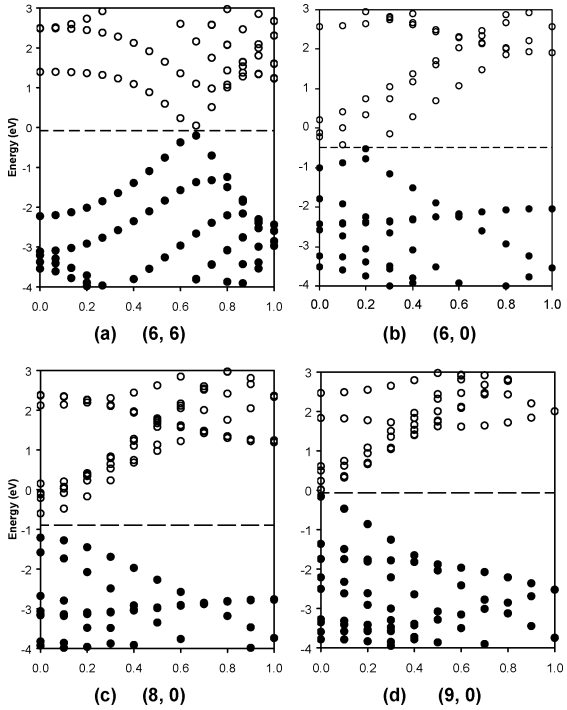


**Figure 6.** Predicted band structures of (6, 6), (6, 0), (8, 0), and (9, 0) SWNTs by density functional theory. The horizontal axis is in units of $\pi/c$, and the horizontal dashed line is the Fermi level, $E_F$. Filled circles indicate occupied electronic states, and empty circles indicate unoccupied states for neutral SWNTs.

unoccupied band in the $k = 0.2-0.8$ range in the band structure of the (6, 0) nanotube and the lowest unoccupied band in the $k = 0-0.4$ range in the band structure of the (8, 0) tube, as shown in Figure 6b, and c. These lowered bands significantly modify the band gaps of these nanotubes in comparison to the simple tight-binding predictions, as has been reported by Blase et al. for several SWNTs.[4] Consequently, the band gaps in nanotubes (5, 0) and (6, 0) are reduced to zero, thus the (5, 0) and (6, 0) nanotubes are metallic at the current GGA level of theory. The band gaps of nanotubes (7, 0) and (8, 0) are reduced from the $\pi-\pi^*$ gaps of 0.90 and 1.20 eV to the actual band gaps of 0.19 and 0.73 eV, respectively. Similar behavior of the band gaps of some of these zigzag nanotubes has been obtained.[3,4,21] For instance, our calculated values of the gaps for the ($n$, 0) tubes for $n = 6$, 7, 8, and 9 are very close to the LDA values of Blase et al.[4] Earlier studies[2a,3,4,21-23] showed that the nonzero curvature generates small nonzero gaps in the otherwise (by Hückel) zero-gap tubes that are not armchair tubes. For the nonmetallic tubes, the deviations of the actual gaps from the relatively larger predicted $\pi-\pi^*$ tight-binding gap values are due to hybridization between the $\sigma^*$ and $\pi^*$ bands. However, with increasing diameter of the tubes, this effect decreases. Consequently, with increasing diameter, the band gaps of nonmetallic zigzag nanotubes first tend to increase and then decrease.

Figure 6d shows the calculated band structure of (9, 0), where the nondegenerate band mentioned above is slightly above the $\pi^*$ band at $k = 0$. Thus, the overall band gap of the (9, 0) SWNT is the $\pi-\pi^*$ gap (Table 2). Similar band structures are obtained for zigzag nanotubes with diameters larger than that of (9, 0), and their band gaps follow the trend predicted by the Hückel-type simple tight-binding method.

We can divide the $\pi-\pi^*$ gaps of zigzag nanotubes into three groups. The nanotubes with $n = 3i$ have zero or very small $\pi-\pi^*$ gaps, those with $n = 3i + 1$ have nonzero band gaps,

**TABLE 2: Theoretical Band Gaps of Neutral Zigzag SWNTs Calculated by DFT[a]**

| | | overall[b] | | |
|---|---|---|---|---|
| | $\pi-\pi^*$ gap | $n = 3i$ | $n = 3i + 1$ | $n = 3i + 2$ |
| (5, 0) | 0.44 | | | 0.00 |
| (6, 0) | 0.11 | 0.00[c] | | |
| (7, 0) | 0.90 | | 0.19[c] | |
| (8, 0) | 1.20 | | | 0.73[c] |
| (9, 0) | 0.20 | 0.20 | | |
| (10, 0) | 0.88 | | 0.88 | |
| (11, 0) | 1.13 | | | 1.13 |
| (12, 0) | 0.08 | 0.08 | | |
| (13, 0) | 0.73 | | 0.73 | |
| (14, 0) | 0.90 | | | 0.90 |
| (15, 0) | 0.14 | 0.14 | | |
| (16, 0) | 0.61 | | 0.61 | |

[a] All values (in eV) are scaled using a uniform factor of 1.20. [b] Overall predicted band gap. [c] These values are lower than the values of $\pi$-$\pi^*$ gap because of the $\pi-\sigma$ mixing discussed in the text.

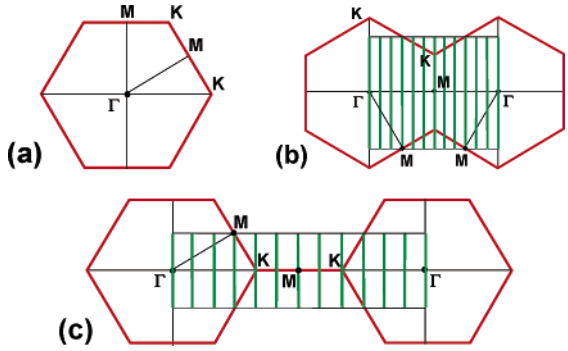


**Figure 7.** (a) Two-dimensional Brillouin zone of graphene and allowed $k$ points of (b) armchair (6, 6) and (c) zigzag (6, 0) SWNTs.

and those with $n = 3i + 2$ have larger band gaps than those for the $n = 3i + 1$ series. This grouping of the gaps into three subgroups within the zigzag tubes is consistent with the observation of the three separate trends discussed for the geometries of zigzag tubes.

The different $\pi-\pi^*$ gaps of the three subgroups is related to the allowed $k$ points in the Brillouin zone.[2] Simply put, there are no restrictions on $k$ values in the $k$ space corresponding to the axis of the tube, but because of the circular boundary conditions, only certain $k$ values are permitted along the direction in $k$ space corresponding to the perimeter of the tube. The allowed $k$ points of any nanotube can be mapped onto the 2D Brillouin zone in the $k$ space of graphene.[2] This mapping exactly connects the states of graphene with those of SWNTs in the simple tight-binding model. The inclusion of $\sigma$ electrons and the breaking of the symmetry between the $b1$ and $b2$ bonds render this mapping only approximate. Figure 7a shows the schematic 2D Brillouin zone of graphene in $k$ space. The K point is where the occupied $\pi$ and the unoccupied $\pi^*$ orbital meet, forming the Fermi level and leading to a zero band gap for graphene.

We consider the frontier (highest occupied and lowest empty) states in the analysis. The line segments in Figure 7b represent the allowed $k$ points for (6, 6), and those in Figure 7c, for (6, 0).[2] When the diameter of the tube is larger, the lines simply become more crowded within the same zone area. Collecting the cross sections of the 2D band structure of graphene produces the band structures for these nanotubes as predicted by the Hückel-type simple tight-binding method.[2] Because the Fermi level of graphene is located at the K point, the band gaps of all types of nanotubes are located at the allowed $k$ points that are

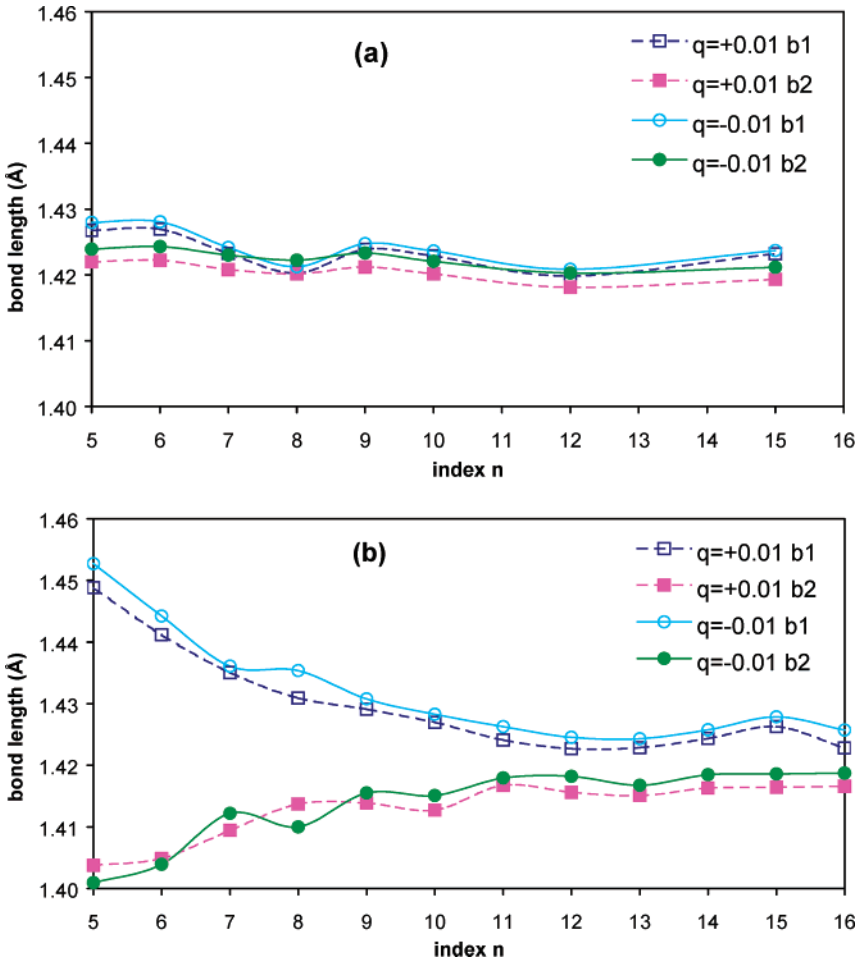


**Figure 8.** Predicted bond lengths in charged (a) armchair ($n$, $n$) and (b) zigzag ($n$, 0) SWNTs. $q$ values refer to electrons per carbon; bonds $b1$ and $b2$ are defined in Figure 2. $q > 0$ corresponds to acceptor doping, and $q < 0$, to donor doping.

either on the K point or closest to it. For armchair nanotubes, because one of the allowed $k$-point lines always goes through the K point, the band gaps are zero in the simple tight-binding method.

For zigzag nanotubes, one of the allowed $k$-point lines goes through the K point when $n = 3i$, thus the band gaps are zero at the Hückel level. None of the lines does so when $n = 3i + 1$ or $3i + 2$; therefore, the band gaps are nonzero at this level. Moreover, the band gaps for nanotubes with $n = 3i + 1$ are located on the MK line in the 2D $k$ space of graphene and on the ΓK line for $n = 3i + 2$. Because the separation between the $\pi$ and $\pi^*$ bands is larger along the ΓK line than along the MK line, the band gaps of the $n = 3i + 2$ series are larger than those of the $n = 3i + 1$ series for the same $i$ value. When the diameter of the nanotube increases, the allowed $k$ point corresponding to the band gap moves closer to the K point, thus the band gap is reduced. The predicted band gaps in Table 2 follow this pattern.

The relatively large band gap of 1.42 eV recently observed[24] in the optical spectrum of individual nanotubes encased in micelles in the samples of the Rice University team corresponds to nanotubes with the smallest diameters of ~7 Å. It appears from our calculations that intrinsic gaps of this order of magnitude may be compatible with the electronic structure of nanotubes with diameters on the order of 8.6 Å. Note that the experiments may refer to chiral tubes but the tubes considered here are all achiral. Other recent experimental progress includes measurements of electronic transitions in semiconducting and metallic SWNTs by both near- and far-IR spectroscopy.[25,26] These measurements result in the band gaps in semiconducting nanotubes[25] and the curvature-induced energy gaps in nonarmchair-like metallic (by Hückel) SWNTs.[26] Direct comparison with our results, however, seems impractical because of the mixture of SWNTs used in the experiment.

### Effect of Small Charge Injection on the Geometries of SWNTs

Charge injection changes the bonding in molecular systems. On the basis of dimensional changes caused by electron transfer to nanotubes, electrodes made from bundles of SWNTs have been recently demonstrated to actuate electromechanically in an electrochemical cell.[27] Detailed calculations aimed at the microscopic interpretation of this effect have been recently described[13] using the same approach as employed in this paper. These calculations were validated on intercalated graphites[13] and doped polyacetylenes[15] and included both counterion-specific and generic (uniform background charge) calculations. In this paper, we show how this charge injection, within the generic model, changes the bonding properties for the four types (armchair and the three series of the zigzag) of nanotubes studied here. Results are summarized in Figure 8; only $q = \pm 0.01e$/carbon ($e$ is the charge of a proton) is considered here.

With a few exceptions for the smaller-diameter tubes, the overall trend is that the bond distances are slightly longer for the negatively charged tubes than for the positively charged ones. The exceptions occur for the zigzag tubes at $n < 9$ and reflect the individuality of tubes with the smallest diameters.

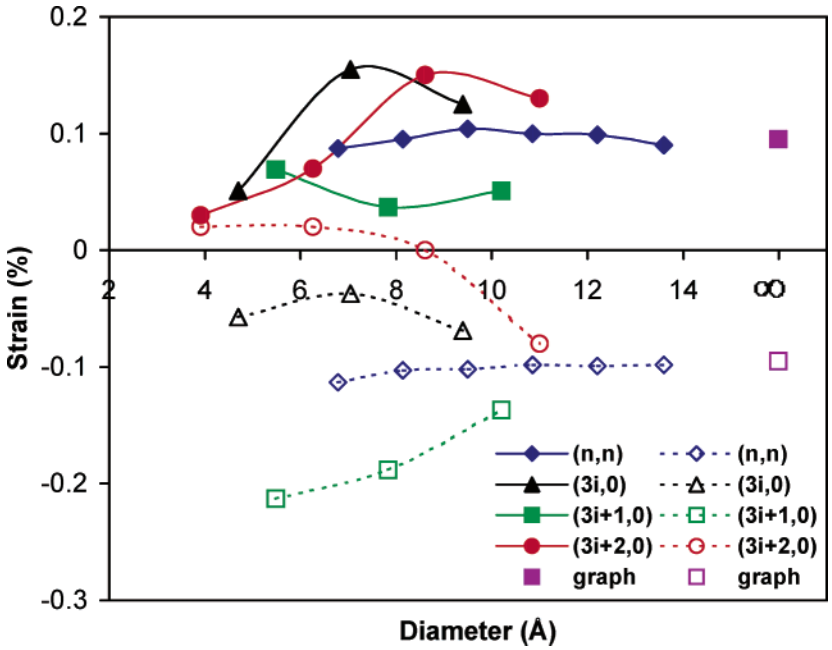


**Figure 9.** Calculated strain as a function of SWNT diameter ($D$) for the four types of nanotubes discussed in the paper. Strain is calculated with respect to the neutral tubes at $q = \pm 0.01e$/carbon charge-injection level. Solid marks and lines refer to $q = -0.01e$, and empty symbols and dashed lines refer to $q = +0.01e$ charge injection. The limiting values calculated for graphene ("graph") are also shown. Strain is defined in eq 2.

These are precisely those tubes that also show special behavior with respect to their band gaps, as discussed above.

We present the results of the same calculations in a different form in Figure 9. Here we show how the strains of the four different series of SWNTs studied in this paper behave as a function of the tube diameter at the two given charge values. Strain is defined as the percentage change of the unit cell length $c(q)$ at $q$ injected charge per carbon:

$$\text{strain}(q) = \frac{100[c(q) - c(0)]}{c(0)} \qquad (2)$$

Two charge values were considered, $q = \pm 0.01e$/carbon. The limiting values for uniformly charged graphene are also given, showing that these graphene values are approached by all four series of SWNTs when the nanotube diameter is large.

The differences in bond lengths are on the order of up to a few $10^{-3}$ Å, in accordance with the fact that the typical charge-induced changes in the lattice constant for intercalated graphites and charged SWCNs are on the order of 0.1% for $q = \pm 0.01e$/carbon.[13] The trend of CC bond elongation for donor doping and shrinking for acceptor doping has been related to the antibonding interactions in carbon networks such as polyacetylene,[28] graphite,[29] and SWNTs.[13,30] At this low charge-injection level, the bond distances already display a diminished undulating pattern as a function of $n$ for the zigzag tubes and, to a lesser degree, for the armchair tubes.

The anisotropic deformations generated by charge transfer have been studied for SWNTs by ab initio[13] and by tight-binding analytical methods.[30] The advantage of the ab initio approach is the high level of accuracy, and the analytical method can be easily applied to any tube, regardless of the unit cell size or chirality of the tube. In both cases, the electron−hole symmetry is broken by second neighbor interactions, an effect that nanotubes "inherited" from graphene.[29] This leads to a strain response with different signs for donor and acceptor doping.

## Conclusions

Density functional theory has been used to predict geometrical and electronic variations of SWNTs as a function of their diameter and charge injection. The undulating patterns observed as a function of tube diameter for the calculated bond distances and unit cell dimensions of the zigzag ($n$, 0) nanotubes lead to three distinguishable subgroups corresponding to $n = 3i$, $3i + 1$, and $3i + 2$. The existence of these three groups is related to the mapping of their frontier electronic states to the states of graphene. The differences among all tubes diminish as the diameter is increased, but for tubes with a diameter as large as 12 Å, significant deviations from graphenelike behavior remain. The geometrical parameters of armchair ($n$, $n$) nanotubes are predicted to be similar to those of graphene.

The band gaps of the small-diameter zigzag tubes that would be metallic in Hückel theory are small but nonzero by the current approach. For nonmetallic zigzag tubes, the band gaps exhibit first an increasing and then a decreasing trend as a function of the tube diameter because of the $\sigma-\pi$ mixing that diminishes as the surface of the tubes becomes more planar with increasing diameter. Again, the three types of zigzag ($n$, 0) tubes ($n = 3i$, $3i + 1$, and $3i + 2$) can be recognized as separate subgroups of nanotubes.

The amplitudes of these undulations are reduced in the charged tubes. From the perspective of the strain response to injected charge, the three subgroups of the zigzag ($n$, 0) tubes behave differently, indicating that they belong to a different series of molecules. The armchair tubes belong to a fourth type of strain−charge behavior that most closely resembles that of graphene. Large deviations from graphenelike strain values are obtained for very small diameter nanotubes. The strain response averaged over various tube types and diameters might be quite close to the strain value obtained for graphene. Small-diameter SWNTs behave as distinctly different molecules with different geometrical and electronic structure parameters.

**Acknowledgment.** Financial support from the National Science Foundation (grants CHEM-9802300 and CHEM-

9601976) and from the Defense Advanced Research Projects Agency (grants N00173-99-2000 and MDA 972-02-C-0005) is gratefully acknowledged. Additional support for R.H.B. from the Robert A. Welch Foundation is gratefully acknowledged. Work in Hungary was supported by grants FKFP-0144/2000 and OTKA-T038014. We thank Professor Siegmar Roth for his enlightening comments.

## References and Notes

(1) Iijima, S. *Nature* **1991**, *354*, 56.

(2) (a) Hamada, N.; Sawada, S.; Oshiyama, A. *Phys. Rev. Lett.* **1992**, *68*, 1579. (b) Mintmire, J. W.; White, C. T. *Carbon* **1995**, *33*, 893. (c) Saito, R.; Fujita, M.; Dresselhaus, G.; Dresselhaus, M. S. *Phys. Rev. B* **1992**, *46*, 1804. (d) Saito, R.; Dresselhaus, G.; Dresselhaus, M. S. *Physical Properties of Carbon Nanotubes*; Imperial College Press: London, 1998.

(3) Kanamitsu, K.; Saito, S. *J. Phys. Soc. Jpn.* **2002**, *71*, 483.

(4) Blase, X.; Benedict, L. X.; Shirley, E. L.; Louie, S. G. *Phys. Rev. Lett.* **1994**, *72*, 1878.

(5) Reich, S.; Thomsen, C.; Ordejon, P. *Phys. Rev. B* **2002**, *65*, 155411.

(6) Perdew, J. P.; Wang, Y. *Phys. Rev. B* **1992**, *45*, 13244.

(7) Vanderbilt, D. *Phys. Rev. B* **1990**, *41*, 7892.

(8) Kresse, G.; Furthmüller, J. *Phys. Rev. B* **1996**, *54*, 11169.

(9) Kresse, G.; Hafner, J. *Phys. Rev. B* **1993**, *47*, R558.

(10) Sun, G.; Kürti, J.; Rajczy, P.; Kertesz, M.; Hafner, J.; Kresse, G. *J. Mol. Struct.: THEOCHEM* **2003**, *624*, 37.

(11) Kresse, G.; Furthmüller, J.; Hafner, J. *Europhys Lett*. **1995**, *32*, 729.

(12) (a) Kürti, J.; Kresse, G.; Kuzmany, H. *Phys. Rev. B* **1998**, *58*, 8869. (b) Milnera, M.; Kürti, J.; Hulman, M.; Kuzmany, H. *Phys. Rev. Lett.* **2000**, *84*, 1324.

(13) (a) Sun, G.; Kertesz, M.; Kürti, J.; Baughman, R. H. *Polym. Mater. Sci. Eng.* **2000**, *83*, 519. (b) Sun, G.; Kürti, J.; Kertesz, M.; Baughman, R. H. *J. Am. Chem. Soc.* **2002**, *124*, 15076.

(14) Kresse, G. Private communication.

(15) Sun, G.; Kürti, J.; Kertesz, M.; Baughman, R. H. *J. Chem. Phys.* **2002**, *117*, 7691.

(16) Choi, C. H.; Kertesz, M.; Karpfen, A. *J. Chem. Phys*. **1997**, *107*, 6712

(17) Wells, A. F. *Structural Inorganic Chemistry*; Clarendon Press: Oxford, U.K., 1987; p 922.

(18) See, for example, Dresselhaus, M. S.; Dresselhaus, G.; Ecklund, P. C. *Science of Fullerenes and Nanotubes*; Academic Press: San Diego, CA, 1996; Chapter 13.

(19) Haddon, R. C.; Scott, L. T. *Pure Appl. Chem*. **1986**, *58*, 137.

(20) Niyogi, S.; Hamon, M. A.; Hu, H.; Zhao, B.; Bhowmik, P.; Sen, R.; Itkis, M. E.; Haddon, R. C. *Acc. Chem. Res*. **2002**, *35*, 1105.

(21) Cao, J. X.; Yan, X. H.; Ding, J. W.; Wang, D. L. *J. Phys. Condens. Matter* **2001**, *13*, L217.

(22) Kane, C. L.; Mele, E. J. *Phys. Rev. Lett*. **1997**, *78*, 1932. Kleiner, A.; Eggert, S. *Phys. Rev. B* **2001**, *63*, 073408.

(23) Kleiner, A.; Eggert, S. *Phys. Rev. B* **2001**, *64*, 113402.

(24) O'Connell, M. J.; Bachilo, S. M.; Huffman, C. B.; Moore, V. C.; Strano, M. S.; Haroz, E. H.; Rialon, K. L.; Boul, P. J.; Noon, W. H.; Kittrell, C.; Ma, J. P.; Hauge, R. H.; Weisman, R. B.; Smalley, R. E. *Science* **2002**, *297*, 593.

(25) Hamon, M. A.; Itkis, M. E.; Niyogi, S.; Alvaraez, T.; Kuper, C.; Menon, M.; Haddon, R. C. *J. Am. Chem. Soc.* **2001**, *123*, 11292.

(26) Itkis, M. E.; Niyogi, S.; Meng, M. E.; Hamon, M. A.; Hu, H.; Haddon, R. C. *Nano Lett.* **2002**, *2*, 155.

(27) Baughman, R. H.; Cui, C. X.; Zakhidov, A. A.; Iqbal, Z.; Barisci, J. N.; Spinks, G. M.; Wallace, G. G.; Mazzoldi, A.; De Rossi, D.; Rinzler, A. G.; Jaschinski, O.; Roth, S.; Kertesz, M. *Science* **1999**, *284*, 1340.

(28) (a) Kertesz, M.; Vonderviszt, F.; Pekker, S. *Chem. Phys. Lett.* **1982**, *90*, 430. (b) Hong, S. Y.; Kertesz, M. *Phys. Rev. Lett.* **1990**, *64*, 3031.

(29) (a) Kertesz, M.; Vonderviszt, F.; Hoffmann, R. In *Intercalated Graphites*; Dresselhaus, M. S., Dresselhaus, G., Fischer, J. E., Moran, M. J., Eds.; North-Holland: New York, 1983; p 141. (b) Kertesz, M. *Mol. Cryst. Liq. Cryst.* **1985**, *126*, 103.

(30) (a) Gartstein, Y. N.; Zakhidov, A.; Baughman, R. H. *Phys. Rev. Lett*. **2002**, *89*, 045503. (b) Gartstein, Y. N.; Zakhidov, A.; Baughman, R. H. *Phys. Rev. B*, submitted for publication. (c) Verissimo-Alves, M.; Koiller, B.; Chacham, H.; Capaz, R. B. *Phys. Rev. B* **2003**, *67*, 161401.